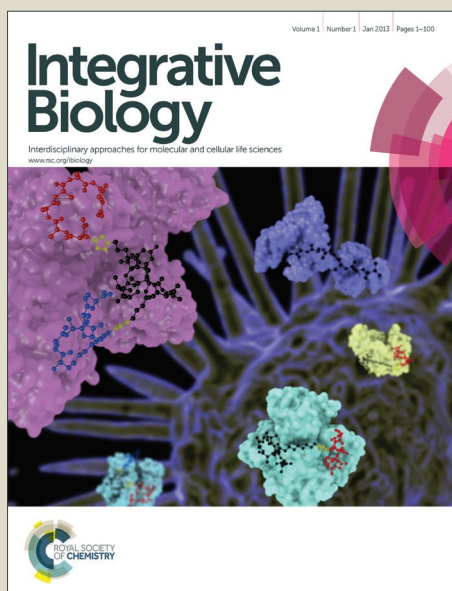


Integrative Biology

Accepted Manuscript



This is an *Accepted Manuscript*, which has been through the Royal Society of Chemistry peer review process and has been accepted for publication.

Accepted Manuscripts are published online shortly after acceptance, before technical editing, formatting and proof reading. Using this free service, authors can make their results available to the community, in citable form, before we publish the edited article. We will replace this *Accepted Manuscript* with the edited and formatted *Advance Article* as soon as it is available.

You can find more information about *Accepted Manuscripts* in the [Information for Authors](#).

Please note that technical editing may introduce minor changes to the text and/or graphics, which may alter content. The journal's standard [Terms & Conditions](#) and the [Ethical guidelines](#) still apply. In no event shall the Royal Society of Chemistry be held responsible for any errors or omissions in this *Accepted Manuscript* or any consequences arising from the use of any information it contains.

Insight Box: Fingerlike projections called villi amplify the surface area of the intestine to permit efficient nutrient absorption. In the mouse, villus formation involves precise folding of a thick pseudostratified epithelium into a series of individual villus domains. The process is extremely rapid; boundaries of individual villi are determined on the timescale of several minutes. In this study, we provide novel insight into this complex morphogenic process by developing a predictive computational model of cytoskeletal force-generated fold formation that is based on *in vivo* observations. This model explains how patterning cues are transferred from the underlying mesenchyme to the overlying epithelium and cause rapid morphogenic changes to the overlying epithelial structure that define the boundaries of the first villi.

1 Coordination of signaling and tissue mechanics during morphogenesis of murine
2 intestinal villi: a role for mitotic cell rounding

3
4 Andrew M Freddo¹, Suzanne K Shoffner², Yue Shao³, Kenichiro Taniguchi¹, Ann S
5 Grosse⁴, Margaux N Guysinger¹, Sha Wang¹, Shiva Rudraraju³, Benjamin
6 Margolis⁵, Krishna Garikipati^{3,6}, Santiago Schnell^{2,7}, Deborah L Gumucio¹

7
8 1. Department of Cell and Developmental Biology, University of Michigan Medical
9 School, Ann Arbor, MI 48109

10 2. Department of Molecular and Integrative Physiology, University of Michigan Medical
11 School, Ann Arbor, MI 48105

12 3. Department of Mechanical Engineering, University of Michigan, Ann Arbor, MI
13 48109

14 4. Charles River Laboratories, Wilmington, MA 01887

15 5. Department of Internal Medicine, University of Michigan Medical School, Ann Arbor,
16 MI 48109

17 6. Department of Mathematics, University of Michigan, Ann Arbor, MI 48109

18 7. Department of Computational Medicine and Bioinformatics, University of Michigan
19 Medical School, Ann Arbor, MI 48015

20
21 **Abstract:** Efficient digestion and absorption of nutrients by the intestine requires a very
22 large apical surface area, a feature that is enhanced by the presence of villi, fingerlike
23 epithelial projections that extend into the lumen. Prior to villus formation, the epithelium
24 is a thick pseudostratified layer. In mice, villus formation begins at embryonic day
25 (E)14.5, when clusters of mesenchymal cells form just beneath the thick epithelium. At
26 this time, analysis of the flat luminal surface reveals a regular pattern of short apical
27 membrane invaginations that form in regions of the epithelium that lie in between the
28 mesenchymal clusters. Apical invaginations begin in the proximal intestine and spread
29 distally, deepening with time. Interestingly, mitotically rounded cells are frequently
30 associated with these invaginations. These mitotic cells are located at the tips of the
31 invaginating membrane (internalized within the epithelium), rather than adjacent to the
32 apical surface. Further investigation of epithelial changes during membrane invagination
33 reveals that epithelial cells located between mesenchymal clusters experience a

34 circumferential compression, as epithelial cells above each cluster shorten and widen.
35 Using a computational model, we examined whether such forces are sufficient to cause
36 apical invaginations. Simulations and *in vivo* data reveal that proper apical membrane
37 invagination involves intraepithelial compressive forces, mitotic cell rounding in the
38 compressed regions and apico-basal contraction of the dividing cell. Together, these data
39 establish a new model that explains how signaling events intersect with tissue forces to
40 pattern apical membrane invaginations that define the villus boundaries.

41

42 **Introduction**

43 The intestine requires an enormous surface area for effective nutrient absorption.
44 Multiple morphological adaptations contribute to this large absorptive surface, including
45 the remarkable length of the intestine (2-4 meters in humans),¹ convolution of its mucosa
46 into fingerlike projections known as villi,²⁻⁴ and the presence of thousands of microvilli
47 on the apical surface of each epithelial cell.⁵ Factors that severely reduce intestinal
48 absorptive surface, whether due to congenital (e.g., short bowel syndrome, microvillus
49 atrophy) or traumatic (e.g., necrotizing enterocolitis, volvulus) etiologies can result in
50 intestinal failure, a life-threatening condition for which there are few treatment options.⁶⁻⁸

51 The presence of villi has been estimated to provide a 6.5-fold amplification of
52 intestinal surface area in humans.¹ Interestingly, the number of villi appears to be largely
53 established by the time of birth; in rodent models of intestinal resection, adaptation
54 consists largely of growth in villus length and girth with little increase in villus number.⁹⁻

55 ¹¹ Thus, the active generation of villi that occurs in fetal life provides the best opportunity

56 for investigation of the morphogenic and molecular pathways required for villus
57 formation.

58 In mice, the first intestinal villi emerge at embryonic day (E)14.5. At this time, the
59 epithelium is over 50 μm thick with nuclei located at staggered positions, a feature that
60 led early investigators to conclude that the epithelium is stratified.^{2,4,12} Furthermore, it
61 was thought that villus domains are established via changes in epithelial cell polarity that
62 result in the formation of *de novo* secondary lumens between cell layers and subsequent
63 fusion of these isolated lumens with the primary lumen.² These long-held notions of
64 villus morphogenesis have recently been dispelled; new evidence from 3D imaging
65 studies reveals a single-layered pseudostratified epithelium with no evidence for
66 disconnected secondary lumens.¹³

67 It is well established that villus formation involves signaling cross-talk between
68 the intestinal epithelium and the underlying mesenchyme.¹³⁻¹⁶ One of the key signals for
69 initiating villus formation is Hedgehog (Hh). Hh ligands secreted from the epithelium
70 stimulate nearby mesenchymal cells to form clusters beneath and closely associated with
71 the epithelium.¹⁵⁻¹⁷ These clusters form in a patterned array, beginning in the duodenum
72 and spreading distally, towards the colon; their pattern appears to be controlled by a self-
73 organizing Turing field that depends on Bmp signaling.¹⁷ Importantly, while Bmp signals
74 organize the distribution of mesenchymal clusters, patterning of the villus boundaries in
75 the overlying epithelium is independent of Bmp signal transduction by epithelial cells.¹⁷
76 Therefore, additional components are required to explain how villus domains are defined
77 in the epithelium.

78 It is also important to consider the speed of villus demarcation. In the mouse, it
79 takes approximately 36 hours (from E14.5 to E16.0) for the initial wave of clusters to
80 propagate from pylorus to cecum.¹⁶ Because the intestine is 30 mm long at E15.5, this
81 morphogenic wave must move at a speed of over 800 μm per hour, nearly 15 μm per
82 minute.

83 To begin to address the mechanisms by which the thick pseudostratified
84 epithelium could be rapidly parsed into separate villus domains, we examined the earliest
85 apical surface deformations in the intestinal epithelium and detected a patterned array of
86 short apical membrane invaginations, or folds, that initiate proximally and spread distally,
87 deepening with time. These folds, which represent the first signs of villus morphogenesis,
88 form predominantly in regions of the epithelium that are not in direct contact with the
89 pre-existing mesenchymal clusters.

90 Further investigation of these initial apical deformations reveals that they are
91 frequently associated with the presence of rounded mitotic cells, suggesting a relationship
92 between cell division and villus morphogenesis. Cell divisions play an important role in
93 apical expansion in at least two other *in vivo* systems: the developing zebrafish neural
94 keel, where apical polarization during cell division establishes the central lumen^{18,19} and
95 formation of the *Drosophila* tracheal placode, where mitotic cell rounding facilitates
96 rapid invagination of epithelial regions that are under passive circumferential
97 compression.^{20,21} We therefore tested whether either of these two models could explain
98 the invaginations associated with villus morphogenesis in the developing intestinal
99 epithelium.

100 We show here that the process of villus morphogenesis closely resembles tracheal

101 placode invagination from morphological, temporal, and mechanical perspectives. We
102 identify epithelial cell shape changes adjacent to mesenchymal clusters that can exert
103 patterned intraepithelial pressure to initiate apical invaginations. We further demonstrate
104 a robust association between apical invaginations and mitotic cells; these cells undergo
105 “internalized cell rounding”, a process by which mitosis-associated cell rounding is
106 accompanied by rapid depression of the apical surface.^{21,22} These *in vivo* observations
107 were used to develop a computational model that allowed further exploration of the
108 mechanical forces required for apical invagination.

109 Together, our data suggest a new model for villus morphogenesis, in which
110 signaling events, initiated by a regular array of mesenchymal clusters, produce a pattern
111 of intraepithelial mechanical forces that, when triggered by mitotic cells, promote rapid
112 apical invaginations. This model establishes a mechanism by which a mesenchymal
113 pattern can be rapidly transferred to the epithelium to establish villus boundaries.

114

115 **Materials and Methods**

116 Mice

117 All protocols for mouse experiments were approved by the University of Michigan Unit
118 for Laboratory Animal Medicine. Animals were maintained in accordance with the
119 guidelines of the University of Michigan, Ann Arbor, Michigan, and all applicable
120 federal, state, local, and institutional laws, regulations, policies, principles, and standards
121 (including accreditation) governing animal research. All protocols for mouse experiments
122 were approved by the University of Michigan Unit for Laboratory Animal
123 Medicine. C57BL/6 mice were obtained from Charles River (strain 027).

124

125 Intestinal Explant Culture

126 Intestines were harvested between E13.5 and E14.5 and dissected in cold DPBS (Sigma
127 D8537). Culturing was performed utilizing transwells (Costar 3428) as a scaffold. BGJb
128 media (Invitrogen 12591-038) containing 1% penicillin-streptomycin (vol/vol)
129 (Invitrogen 15140-122) and 0.1 mg/mL ascorbic acid was placed into contact with the
130 transwell membrane. Intestines were cultured for up to 24 hours at 37°C with 5% CO₂.

131

132 Antibodies, Plasmids, and Reagents

133 Antibodies used were rabbit anti-aPKC 1:250 (Santa Cruz sc-216), mouse anti- α -tubulin
134 1:1000 (Sigma T6199), mouse anti- β -catenin 1:500 (Sigma C-7207), rabbit anti-cleaved
135 caspase 3 1:150 (Cell Signaling 9664), rabbit anti-Crumbs3 1:250 (gift of Dr. Ben
136 Margolis), mouse anti-E-cadherin 1:1000 (Invitrogen 13-1900), mouse anti-Ezrin 1:1500
137 (Sigma E8897), rabbit anti-Ki67 1:500 (Novocastra NCL-Ki67p), rabbit anti-pMLCK
138 1:200 (Cell Signaling 3674), rabbit anti-PDGFR α 1:200 (Santa Cruz sc-338), mouse anti-
139 pHH3 1:1000 (Millipore 05-806), rabbit anti-pHH3 1:1000 (Millipore 06-570).
140 Secondary antibodies used were Alexa Fluor 488/555/647-conjugated anti-mouse and
141 anti-rabbit and Alexa Fluor 568 Phalloidin (Life Technologies A34055).

142

143 Tissue Immunofluorescence

144 After fixing overnight in 4% paraformaldehyde in PBS at 4°C, intestines were washed in
145 PBS, embedded in paraffin, and sectioned at 5 μ m. Samples were deparaffinized and 10

146 mM sodium citrate used for antigen retrieval. Primary antibody incubation was
147 performed overnight at 4°C, followed by secondary antibody for 30 minutes at room
148 temperature. Samples were imaged on a Nikon E800 (20x objective) and a Nikon A1
149 Confocal (20x objective, water; 60x objective, oil). Adobe Photoshop was used for image
150 processing.

151

152 Vibratome Sectioning and Immunofluorescence

153 After fixation, intestines were embedded in 7% (wt/vol) low-melting agarose (Sigma
154 A9414) in PBS and sectioned at 100 µm. Primary antibody incubation was performed
155 overnight at 4°C, followed by secondary antibody incubation for two hours at room
156 temperature. Samples were mounted in Prolong Gold (Life Technologies P36930) and
157 imaged on a Nikon A1 Confocal (20x objective, water). Image processing was done
158 using Imaris 8.0.

159

160 Scanning Electron Microscopy

161 After harvest, intestines were fixed at 4°C in 2.5% glutaraldehyde overnight and washed
162 in Sorenson's phosphate buffer (0.1 M, pH 7.4). Overnight treatment with
163 hexamethyldisilazane was followed by mounting and sputter coating with gold. An
164 Amray 1910 FE Scanning Electron Microscope was used to examine samples, with
165 images taken using Semicaps 2000 software. Image processing was done using Adobe
166 Photoshop.

167

168 Computational Model

169 Modeling was done using the finite element method (FEM), which is a mesh based
170 discretization technique for solving partial differential equations.²³ The computational
171 results in this paper were generated using the FEM package Abaqus (version 6.14.1),
172 which was used to solve the equations governing the mechanical deformation of the
173 epithelium. The pre-villus epithelium was modeled as a 2D geometry (Supplementary
174 Figure 3) and we assumed a hyper-elastic Holzapfel-Gasser-Ogden material model with
175 spatially varying material properties (Supplementary Table 1).

176

177 Statistical Analysis

178 All graphs were made and statistical analyses performed using Prism 6. Statistical tests
179 were used as indicated in the figure legends.

180

181 **Results**

182 Apical expansion during villus morphogenesis

183 We previously documented that villus morphogenesis involves expansion of the
184 main lumen rather than formation and fusion of disconnected secondary lumens.¹³ To
185 further explore the initial changes in the apical surface that accompany this expansion, we
186 examined this process in E13.5 to E15.5 intestines utilizing antibodies to EZRIN, an
187 apical surface protein,²⁴ and PDGFR α , a marker of the mesenchymal clusters involved in
188 villus patterning.¹⁶ Both cross sections (Figure 1A-C) and longitudinal sections (Figure
189 1D-F) of tissue were examined.

190 At E13.5, the epithelium is uniformly pseudostratified and the apical surface is
191 flat; mesenchymal clusters are not detectable (Figure 1A and D). At E14.5, mesenchymal

192 clusters are visible in the proximal, but not distal intestine. Clusters are tightly associated
193 with the overlying epithelium, sitting in small alcoves and slightly deforming the basal
194 surface of the pseudostratified epithelium (Figure 1B and E, asterisks). The apical
195 surface, however, remains flat, with occasional short extensions of EZRIN staining
196 oriented perpendicularly to the luminal surface in the proximal intestine (Figure 1B and
197 E, arrows). By E15.5, these apical extensions are deeper and a field of regularly patterned
198 villi cover the proximal intestine, such that each villus is closely associated with a
199 mesenchymal cluster (Figure 1C and F). All of these events first occur in the proximal
200 intestine and, after about one day, are present distally, consistent with previous findings
201 that villus formation occurs in a proximal to distal wave.^{2,16}

202

203 *Spatiotemporal characterization of apical lumen expansion*

204 The spatial patterning of EZRIN positive apical extensions was then examined.
205 These experiments were performed using an intestinal explant culture; in such explants,
206 the rate of villus morphogenesis slows, allowing greater resolution of the morphogenic
207 process.¹⁶ The location of apical extensions relative to mesenchymal clusters was
208 quantified. In the proximal E14.5 and distal E15.5 intestine, where the morphogenic front
209 of villus emergence is located, over 80% of the apical deformations are found in
210 epithelial regions that lie between, rather than over clusters (Figure 1G).

211 A spatiotemporal correlation was also apparent between the depth of apical
212 extensions and their location along the proximal-distal axis: at E15.0, midway through
213 the morphogenic process, these indentations are deeper in the proximal compared with
214 distal regions of the same intestine (Figure 1H). This mirrors the established pattern of

215 cluster formation, as clusters first form in the proximal duodenum and spread in a wave-
216 like fashion down the intestine over a 36 hour period (E14.5 to E16.0).¹⁶ Because clusters
217 are known to mark the core of villus domains,¹⁶ these short apical extensions appear to
218 represent the initial boundaries between villi.

219

220 Three-dimensional visualization of apical surface changes

221 To better understand the three-dimensional structure and pattern of apical surface
222 extensions during initial villus demarcation, two approaches were taken. First, thick (100
223 μm) vibratome sections were stained with phalloidin to mark the apical F-actin network.
224 Confocal Z stacks were generated and reconstructed in three dimensions to determine the
225 shape of individual extensions (Figure 2A-B). These studies establish that the smallest
226 extensions consist of closely opposed double-membrane folds or invaginations, with little
227 luminal space between membranes. Importantly, as these folds deepen, they remain
228 continuous with the apical surface. Previous work has established that the apical surface
229 remains continuous throughout villus development.¹³

230 To further appreciate the patterning of these invaginations, intestines from
231 embryos ranging from E14.0 to E14.5 were longitudinally opened and scanning electron
232 microscopy (SEM) was used to image the apical surface. In E14.0 intestines, the surface
233 is flat, though cellular outlines are visible (Figure 2C). Beginning in the duodenum at
234 E14.5, a dramatic transition can be observed along the proximal to distal axis; domes
235 surrounded by deep creases are located more proximally to areas of disconnected
236 invaginations (Figure 2D). The field seen in this image, which appears to represent the
237 transitional front of the morphogenic wave, measures slightly more than 150 μm .

238 Assuming that this wave moves at a constant speed between E14.5 and E15.5, we
239 calculate that the entire morphological transition (from right to left) that is pictured in
240 Figure 2D should take place in about 10 minutes.

241

242 *Apical surfaces are not extended by apoptosis*

243 The data above indicate that apical invaginations appear beginning at E14.5 in a
244 spatiotemporally controlled pattern in the developing intestine and that these
245 invaginations are likely nascent villus demarcations. We next sought a mechanism to
246 explain the appearance of these invaginations. During morphogenesis of the *Drosophila*
247 leg, apoptosis facilitates epithelial folding by coupling cell death to the transmission of
248 physical forces.²⁵ Additionally, in the early neural ectoderm, apoptosis generates force to
249 assist tissue bending before neural tube closure.^{26,27} To determine whether localized
250 apoptosis might cause apical folding during villus morphogenesis, we examined the
251 pattern of cleaved Caspase 3 staining in E14.5 intestines. This analysis revealed that the
252 frequency of apoptosis is very low both before and during villus morphogenesis
253 (Supplementary Figure 1). The rare apoptotic figures scattered throughout the epithelium
254 do not appear to correspond with apical surface extensions or mesenchymal clusters.
255 Therefore, the establishment of villus domains is not determined by localized patterns of
256 apoptosis.

257

258 *Apical folds are associated with dividing cells*

259 Another event that has been associated with the generation of new apical surfaces
260 is mitosis.^{18,19,21,22,28-30} We therefore examined the distribution of dividing epithelial cells

261 during the process of apical expansion. Interestingly, 40% of pHH3+ mitotic figures were
262 found at the tips of invaginations (Figure 3A-B). This association is remarkable
263 considering that the tips of these folds constitute a small proportion of the total apical
264 surface (Figure 3A). Moreover, approximately 60% of folds have an associated cell
265 division (Figure 3C).

266 Because these data suggest a potential mechanistic link between mitotic cells and
267 membrane invaginations, we examined two mechanisms by which mitotic cells promote
268 apical expansion in other systems. First, a new luminal surface can form *de novo*
269 between daughter cells during cell division; this happens in the zebrafish neural keel,^{18,19}
270 in the formation of bile canaliculi *in vitro* and *in vivo*,²⁸ and in isolated epithelial cells
271 plated in a thick 3D matrix.^{29,30} Alternatively, cell division can accelerate the process of
272 apical invagination, as in the *Drosophila* tracheal placode.²¹

273

274 *Dividing cells at folds are not enriched for apical components*

275 In lumen-forming cell divisions, intracellular collections of apical components
276 such as CRB3 and Pard3 are observed at the two poles of the dividing cells. During
277 cytokinesis, these components traffic along the mitotic spindle to initiate lumen formation
278 between daughter pronuclei.^{18,19,29} To examine CRB3 distribution during cell division in
279 the intestinal epithelium, we studied its localization in sections co-stained with α -
280 TUBULIN (Supplementary Figure 2). No intracellular staining was found in the 30
281 divisions examined. Though not definitive, these data suggest that the mitotic cells at
282 apical invaginations are not likely to be generating apical surfaces *de novo*. Thus, we

283 explored whether mitosis-associated invagination could provide an explanation for
284 luminal expansion, as in the *Drosophila* tracheal placode.

285

286 *Apical intestinal invagination resembles Drosophila tracheal placode invagination*

287 Prior to invagination in the *Drosophila* tracheal placode, intercalating cells around
288 the presumptive placode expand the surrounding epithelium, placing a passive
289 intraepithelial compressive force on placode cells. As described by Kondo and Hayashi,
290 as a cell within this compressed region begins mitosis, the circumferential pressure
291 causes its apical contact to shrink and the rounded cell moves away from the apical
292 surface while retaining a T-shaped apical extension (Supplementary Figure 8 in Kondo
293 and Hayashi²¹). This is referred to as “internalized cell rounding” and is distinct from
294 surface cell rounding that typically characterizes mitosis in a pseudostratified epithelium.
295 Overall, these events cause a rapid inward folding of the apical surface. The defining
296 morphological and physical characteristics of this model include the presence of
297 internalized mitotic cell rounding and a source of patterned intraepithelial pressure.^{20,21}

298 Examination of rounded mitotic cells in the intestinal epithelium at E14.5 and
299 E15.5 revealed two distinct morphologies. Mitotic cells that are not associated with apical
300 invaginations round up directly adjacent to the main luminal surface, as expected in a
301 pseudostratified epithelium (Figure 4A, asterisk). Some of these cells are associated with
302 a small V-shaped indentation of the apical surface (Figure 4B), although internalized cell
303 rounding is not observed. In contrast, rounded mitotic cells associated with initial apical
304 invaginations are positioned well below the apical surface and are connected to the main
305 lumen by a short T-shaped apical fold that stains with apical markers such as EZRIN. The

306 rounded cell retains a very small EZRIN-positive apical surface at the tip of the
307 invagination (Figure 4A, C). These cells are morphologically indistinguishable from
308 those previously noted in the *Drosophila* tracheal placode. Such internally rounded cells
309 cannot be detected prior to cluster formation at E14.5.

310 Tracheal placode invagination takes place in the context of passive compression
311 of presumptive placode cells due to expansion of the surrounding epithelium.²¹ If a
312 similar process occurs in the intestinal epithelium, a source of compressive pressure is
313 required. Because initial intestinal invaginations are consistently located between clusters
314 (Figure 1G), an attractive hypothesis is that a cluster-dependent pattern of intraepithelial
315 compression is generated. As demonstrated above, analysis of the epithelium prior to
316 apical invagination reveals that the basal surface of the epithelium is deformed into soft
317 alcoves above the clusters, even while the apical surface remains flat (Figures 1E, 2C-D,
318 3A, 4A, 5A-C and 5G). As pointed out in a previous study¹⁷ all of these soft alcoves are
319 associated with the presence of mesenchymal clusters, suggesting that the clusters form
320 these deformations. Early investigators noted this deformation as well and suggested that
321 clusters “push up” into the overlying epithelium.² However, another plausible explanation
322 for these basal deformations could be that clusters signal to overlying epithelial cells to
323 cause them to change shape. Indeed, measurements show that epithelial cells overlying
324 clusters are up to 30% shorter than those in the inter-cluster regions at a time when
325 minimal to no deformation is detectable at the apical surface (Figure 5D). Though the
326 “cluster push” hypothesis is not ruled out by these findings, such pushing would also
327 require a motor force as well as a substrate for traction, neither of which has been
328 documented. Together, the bulk of the data presented here and elsewhere^{16,17} support the

329 hypothesis that signals from the clusters cause shape changes in overlying epithelial cells,
330 causing those cells to shorten and widen. Since clusters are known to be tightly
331 associated with the basement membrane¹⁶, they may, in fact, be pulled up by the
332 epithelial shape-induced deformations.

333 To accommodate this basal to apical shortening, cell volume must rapidly
334 decrease, or cells must widen circumferentially. To examine these possibilities, Imaris
335 image analysis software was first used to compare the volume of cells over clusters and
336 between clusters. While individual volume is quite variable, these measurements reveal a
337 similar range of volumes in both locations (Figure 5E), arguing against volume change as
338 a compensation for this rapid change in cell height. Similarly, in other morphogenic
339 systems characterized by rapid cell shape changes, cell volume is constant.³¹⁻³³

340 Because of the non-linear elastic response of the cytoplasm,³⁴ the vertical
341 shortening of these cells would predict a lateral increase in cell width. To determine if
342 this effect is observed in the intestinal epithelium, the number of epithelial cells (nuclei)
343 per unit apical length was determined in regions overlying mesenchymal clusters and in
344 regions between clusters. These measurements revealed a lower density of nuclei per unit
345 of apical surface in regions over clusters, suggesting that cells in this region are indeed
346 wider (Figure 5F). Additionally, we utilized confocal microscopy to image longitudinally
347 opened, whole-mount E15.0 intestines; in this manner the apical surface could be directly
348 examined at the front of the morphogenic wave of clusters. Confocal slices through this
349 epithelium, stained with E-cadherin to mark cell outlines, reveal that epithelial cells
350 directly over clusters are circumferentially expanded, relative to the intervening epithelial
351 cells, which appear more compacted (Figure 5F). Thus, epithelial cell shape changes

352 initiated by the presence of mesenchymal clusters appear to exert a patterned field of
353 compressive forces on the intervening epithelium.

354

355 *Computational model of the mechanics of apical invagination*

356 To explore whether this pattern of forces could potentially explain the patterning
357 and morphology of initial apical folds, a two-dimensional (plane strain) finite element
358 model of the intestine was constructed, using the commercial software Abaqus 6.14.1.
359 The epithelium contains two structural layers with differing mechanical properties: the
360 thin apical layer contains the cross-linked actin-rich cytoskeleton network and the cell
361 body layer represents the rest of the epithelium. In this model, these layers are
362 represented by regions of different mechanical properties (Supplementary Table 1). The
363 geometric dimensions of this model were estimated from previous experimental
364 observations of the developing intestine. The thickness of the pre-villus epithelium has
365 been established to be $50 \mu\text{m}^{13}$ with an apical terminal web of $1 \mu\text{m}^{35}$. Mesenchymal
366 clusters are approximately $30 \mu\text{m}$ wide and $70 \mu\text{m}$ apart.¹⁶ For this reason, $15 \mu\text{m}$ is
367 defined as a half-cluster region for each flanking region of this segment. Because mitotic
368 cells are associated with invaginations *in vivo*, some simulations also included a
369 rectangular region of $10 \mu\text{m}$ by $18 \mu\text{m}$ with an apical contact width of $1 \mu\text{m}$ to represent a
370 mitotic cell. The dimensions of this model are shown in Supplementary Figure 3.

371 The mechanical stiffness of each region of the model was selected based on
372 previous studies. The modulus of the actin-rich apical layer was chosen to be 10 kPa
373 based on the measurements of the Young's modulus of actin stress fibers.³⁶ The modulus
374 of the cell body layer was chosen to be 0.5 kPa based on measurements of the Young's

375 modulus of cytoplasm.³⁴ The epithelial cytoplasm was assumed to be nearly
376 incompressible, with Poisson's ratio of 0.495. During mitotic cell rounding, the apical
377 actin web is disassembled, allowing the cell cortex to be stiffer than the surrounding
378 epithelial cells, such that the dividing cell can displace neighbors to accommodate
379 rounding.³⁷ Therefore, the apical contact of the mitotic cell was modeled as a compliant
380 spot with an 80% reduction in modulus compared with the rest of the apical surface.

381 Because the modeled region represents a repeating unit of the intestinal
382 epithelium, symmetric boundary conditions were used for the left and right boundaries.
383 To model the cluster-mediated cell shortening effects that cause basal deformations, as
384 observed in the *in vivo* developing epithelium, the apical surface above the clusters was
385 constrained vertically such that the clusters would deform only the basal surface of the
386 epithelium. Because the inter-cluster epithelial cells do not shorten, the basal inter-cluster
387 boundary was fixed. These idealized assumptions in the model reflect hypotheses that
388 similar conditions possibly constrain the intestinal epithelium.

389 To mimic the changes in cell shape that occur above mesenchymal clusters, an
390 inelastic growth strain was applied, as is common in mechanical models of growing
391 tissues.^{38,39} Cell signaling leads to the shortening and widening of epithelial cells in the
392 cluster region, which is represented by a growth strain that is positive in the lateral
393 direction and negative in the vertical direction. To model the unchanged thickness of the
394 apical surface during this process, only a positive lateral growth strain was applied to the
395 apical surface above the clusters.

396 In initial simulations, we tested whether cluster-mediated expansion is sufficient
397 to cause apical invaginations in the inter-cluster regions. As shown in Figure 6A

398 (Supplemental Movie 1), when cluster-dependent strain was applied, the apical surface
399 exhibited a wave-like pattern, but no pronounced invagination. Because our *in vivo*
400 observations (Figure 3 and 4) as well as work in the *Drosophila* trachea²¹ suggest that
401 mitotic cells might assist the invagination process, we next modeled a mitotic cell at the
402 apical surface, as a small compliant region (yellow star in Figure 6), to represent
403 cytoskeletal changes (disassembly of the apical actin network) during mitosis. However,
404 no invagination was seen in these simulations (Figure 6B and Supplemental Movie 2),
405 suggesting that another feature is necessary in the model.

406 Kondo and Hayashi report that invagination is associated with downward
407 movement of the rounded mitotic cell into the epithelium, giving rise to internally
408 rounded mitotic cells,²¹ a feature clearly detected in the murine intestine. Recent work in
409 the zebrafish otic primordium further confirms that in a pseudostratified epithelium, at
410 the points of strain, mitotically rounded cells contract along the apical-basal axis.²²
411 Therefore, additional simulations included a negative inelastic growth strain (contraction)
412 applied in the vertical direction to both the small apical contact and the cytoplasmic
413 region containing the cell. Combining these three features (cluster-dependent strain, a
414 compliant apical defect and vertical contraction) results in a fold with closely opposed
415 membrane, similar to the T-shaped folds observed *in vivo* (Figure 6C, Supplemental
416 Movie 3).

417 Finally, to explore whether mitosis (both the compliant apical defect that models
418 rounding and the vertical contraction that accompanies rounding) is sufficient to form
419 invaginations, we ran simulations with these two features alone, but without cluster
420 expansion. Interestingly, in this case, the apical surface deformed with a rounded

421 indentation (Figure 6D, Supplemental Movie 4), reminiscent of the V-shaped folds
422 observed at some dividing cells that are apically located and not associated with
423 invaginations (Figure 4B), and also similar in appearance to mitotic cells that are present
424 prior to clusters formation at E14.5. Together, these simulations suggest that
425 intraepithelial forces produced by cluster-mediated epithelial shape changes and
426 internalized mitotic cell rounding are sufficient to produce apical invaginations that
427 mirror those seen at membrane invaginations *in vivo*.

428

429 *In vivo evidence for enriched actin in basal processes of mitotic cells*

430 As shown in Figure 4C, mitotic cells at apical intestinal folds are reduced in
431 height and “internalized”; they connect to the main luminal surface by a short extension
432 of apically stained membrane, a feature that they share with mitotic cells that facilitate
433 invagination in the *Drosophila* tracheal placode.²¹ Active apical-basal shortening of
434 mitotic cells in the context of the developing otic epithelium has also been demonstrated
435 by Hoijman et al., and in that study, the basal process of the mitotic cell was found to be
436 enriched in filamentous actin.²² Since our computational model predicts that a contraction
437 oriented in the apical-basal direction at the position of the mitotically rounded cell is
438 critical for proper folding, we examined E14.5 and E15.5 intestinal sections stained with
439 phalloidin (which marks F-actin). Enhanced actin staining was indeed detected in the
440 basal processes of cells dividing at invaginations (Figure 7), potentially indicating an
441 active downward force.

442

443 **Discussion**

444 The morphological events involved in villus formation were first described
445 several decades ago. However, the use of thin sections to document the dramatic
446 epithelial changes that occur during this process led to the incorrect conclusions that the
447 early epithelium is stratified and that *de novo* lumen formation is an important feature of
448 villus morphogenesis.^{2,4,12} The work described here utilizes recently redefined parameters
449 regarding intestinal morphogenesis: the epithelium prior to remodeling is a single
450 pseudostratified epithelial cell layer and luminal expansions are invaginations of the
451 apical surface.¹³ Within this revised context, we suggest a new model to account for
452 initial epithelial changes during establishment of the villus domains.

453 We propose that demarcation of the first villi involves formation of patterned
454 epithelial invaginations that, in turn, require inputs from cell-cell signaling events
455 combined with intraepithelial compressive forces. First, Hh signals from the thick
456 pseudostratified epithelium cause sub-epithelial mesenchymal clusters to form.¹⁶ The
457 positioning of these clusters is determined by a self-organizing Turing field mechanism
458 that is driven by mesenchymal Bmp signaling.¹⁷ Over the next 36 hours, these clusters
459 spread in a proximal to distal wave over the length of the intestine.^{16,17} As they form,
460 clusters signal to the overlying epithelium, causing these cells to change shape,
461 shortening in the apical-basal dimension and expanding laterally. We propose that these
462 localized shape changes over the clusters generate an intraepithelial compressive force on
463 cells located between clusters. Within these pressurized regions, mitotic cell rounding
464 causes rapid invagination of the apical surface.

465 This process of mitosis-assisted invagination is faithfully recapitulated by our
466 computational model, demonstrating that intraepithelial mechanical forces are sufficient

467 to result in invaginations similar to those seen *in vivo*. Three features are required to
468 recapitulate the fold structure *in silico*: pressure from expansion of the clusters,
469 compliancy of the apical surface due to cortical actin changes in the rounded cell, and a
470 vertical displacement of the mitotic cell in the apical-basal dimension. Removal of any of
471 these components from the computational model results in a failure of a typical T-like
472 invagination to occur.

473 Overall, the apical invagination accompanying villus morphogenesis shares many
474 features with tracheal placode invagination in *Drosophila*. First, the process is
475 accompanied by a patterned field of intraepithelial forces that place a passive
476 compressive force on the regions that will indent. In the intestine, this compression likely
477 arises from the lateral expansion of epithelial cells over clusters. Second, mitotic cells are
478 associated with invaginations in both cases. Third, these cells have a characteristic
479 appearance in sectioned material, previously defined as “internalized cell rounding.”²¹
480 That is, these cells round up and enter mitosis well beneath the main surface of the
481 epithelium, but remain connected to the lumen by the apical membrane fold. Finally, the
482 process of invagination is very fast in both cases, taking place over a period of minutes.
483 Live cell imaging of *Drosophila* tracheal placode invagination shows that the initiation of
484 mitosis in a cell within the constricted region releases the stored resistance of central cells
485 and results in a rapid invagination.²¹ In the intestine, we propose that similar forces result
486 in the rapid demarcation of villus boundaries.

487 The revised model that we propose here for apical invagination in the mouse
488 relies on the intersection of tissue mechanics with soluble signals to pattern the location
489 of villus domains. The combined action of tissue forces and signaling is also seen during

490 morphogenesis of the chick intestine, but the mechanistic details of that process exhibit
491 interesting differences in chick and mouse. This might not be surprising, as it has been
492 noted that over evolutionary time, villi likely arose independently in birds and mammals
493 as morphological adaptations to assist nutrient absorption.⁴⁰ During “villification” in the
494 chick, mechanical forces from the developing muscle layers actively set the pattern for
495 the eventual location of clusters and villi.⁴¹ Formation of an inner circular smooth muscle
496 deforms the epithelium into longitudinal ridges, and subsequent development of an outer
497 longitudinal layer forces those ridges into zig-zags. These progressive epithelial
498 deformations serve to trap localized maxima of Hh ligand secreted from the epithelium.
499 Hh signals then induce the expression of mesenchymal cluster factors, such as Bmp4,
500 which promote villus emergence from the arms of the zig-zags.^{40,41} Thus, in the chick,
501 mechanical forces establish a pattern of epithelial deformations that then direct, via
502 signaling, the formation of mesenchymal clusters and villi.

503 In contrast, in mammalian species studied to date (mouse, rat, pig, and human),
504 the epithelium never forms zig-zags, though in some cases, a few longitudinal pre-villus
505 ridges are observed.⁴²⁻⁴⁵ Additionally, in the mouse and human, formation of muscle
506 layers does not coincide with villus formation; thus, muscle-induced tension does not
507 play a patterning role.^{17,42,43} Rather, as demonstrated here in the mouse, a patterned field
508 of mesenchymal clusters forms prior to any epithelial deformation, but the presence of
509 these clusters provides subsequent mechanical input to the epithelium. That is, these
510 clusters signal to overlying epithelial cells to promote cell shape changes, thereby
511 creating a pattern of intraepithelial forces that determine where villus boundaries will lie.

512 Elucidating the exact nature of these mesenchymally-derived morphogenic signals will be
513 an important goal for future investigations.

514 It is also noteworthy that by the time villi initiate in the chick, epithelial cells have
515 already adopted a short columnar structure.^{41,46} Indeed, this flexible structure is probably
516 required for effective muscular deformation of the epithelium that is needed to create the
517 deep alcoves that can trap Hh signals.^{40,41} In contrast, mouse villi arise directly from a 50
518 μm thick pseudostratified epithelium. Thus, villus development in the mouse requires a
519 mechanism to quickly fold this thick epithelium in a patterned manner that corresponds
520 with the established pattern of mesenchymal clusters. We propose that the use of mitosis-
521 associated epithelial folding facilitates this transition to rapidly generate the initial villus
522 domains.

523

524 **Acknowledgments**

525 The authors would like to thank the University of Michigan Microscopy and Image
526 Analysis Laboratory for assistance with preparing and imaging samples. We also would
527 like to thank Drs. Linda Samuelson, Jason Spence, Daniel Teitelbaum, Kristen Verhey,
528 Katherine Walton, and Yukiko Yamashita for discussions. Support was provided by NIH
529 F30 DK100125 and the University of Michigan Medical Scientist Training Program
530 (AMF) and NIH R01 DK089933 (DLG).

531

532 **Competing Interests**

533 The authors declare no conflicts of interest

534

535 Author Contributions

536 Contributed to concepts, approaches: AMF, SKS, YS, KT, ASG, SR, KG, SS, BM, DLG

537 Performed experiments: AMF, MNG, SW

538 Performed computations: SKS, YS, SR

539 Analyzed data: AMF, SKS, SR, KG, SS, DLG

540 Prepared the manuscript: AMF, SKS, DLG

541 Edited the manuscript: AMF, SKS, KG, DLG

542

543 Figure Legends

544 **Figure 1. Temporal analysis of the intestinal apical surface during villus initiation.**

545 (A-C) Cross-sections and (D-F) longitudinal sections of the murine small intestine at (A,

546 D) E13.5, (B, E) E14.5, and (C, F) E15.5 stained with EZRIN (green) and PDGFR α

547 (red). Initial deformations appear at E14.5 (B and E, arrows). Mesenchymal clusters are

548 marked with asterisks. Folds deepen to clearly demarcate villi by E15.5. Scale bar = 50

549 μm . (G) Quantification of fold location relative to mesenchymal clusters at the

550 morphogenic front of villus development at E14.5 and E15.5. (H) Box and whisker plots

551 comparing fold depth in the E15.0 proximal and distal intestines showing the maximum,

552 minimum, and median of the data sets ($p = 0.0026$, unpaired t-test).

553

554 **Figure 2. Three-dimensional analysis of apical invaginations.** (A) Reconstruction of

555 the apical surface (phalloidin, red) indicating an early fold located between two clusters

556 (asterisks). Images were obtained by confocal scanning of a 100 μm thick vibratome

557 section of the E14.5 intestine, and the 3D view was reconstructed using Imaris. The

558 basement membrane is traced with a white line. (B) Inset of box in (A), the underside of
559 the apical surface is traced with a white line. The fold represents an invagination of the
560 apical surface; two membrane faces are visible. Scale bar = 10 μm . (C, D) Scanning
561 electron micrographs of the apical surface at E14.0 and E14.5. In both images, proximal
562 is on the left and distal is on the right. (C) At E14.0, although cell boundaries are visible,
563 the overall surface is flat. Occasional larger cell profiles represent mitotic cells
564 (arrowheads). (D) At E14.5, deeper folds (arrows) clearly outline nascent villi. Nearby,
565 shallower, disconnected invaginations (asterisks) are visible. Because the rate of cluster
566 spread is 30 mm over 36 hours, or 15 μm per minute,¹⁶ the morphogenic wave can travel
567 this 150 μm field in approximately 10 minutes. Scale bar = 10 μm .

568

569 **Figure 3. Apical folds are associated with dividing cells.** (A) Cross-section of the
570 intestine stained with pHH3 (green) and phalloidin (red). Many apical folds are
571 associated with mitotic cells (arrows). Note that phalloidin also stains the outer smooth
572 muscle layer and there is some background from antibody trapping in the mesenchymal
573 connective tissue. Scale bar = 50 μm . (B) Quantification of the location of dividing
574 (pHH3+) cells in the epithelium at E14.5. Forty percent of invaginations are associated
575 with a dividing cell. (C) Quantification of the number of folds associated with a dividing
576 cell. Sixty percent of folds are associated with a cell division event. Error bars represent
577 standard deviation.

578

579 **Figure 4. Two types of cell division in the intestinal epithelium.** (A) Cross-section of
580 the intestine at E14.5. A subset of dividing cells (KI67, red) are associated with a T-

581 shaped invagination of the apical surface (arrow). Other rounded mitotic cells are
582 adjacent to a flat or V-shaped (asterisk) surface indentation. Apical surface is stained with
583 antibodies to EZRIN (green). Clusters are also stained with antibodies to PDGFR α (red).
584 Scale bar = 50 μ m. (B, C) Confocal images of dividing cells (KI67 or pHH3, red)
585 adjacent to a (B) V-shaped (asterisk) or (C) T-shaped (arrow) apical indentations
586 (EZRIN, green). This T-shaped indentation is reminiscent of internalized cell rounding
587 described in the *Drosophila* tracheal placode.²¹ Scale bar = 5 μ m.

588

589 **Figure 5. Epithelial cells above mesenchymal clusters are shorter and wider.**

590 (A) Example of the basal epithelial deformation that is created by a small mesenchymal
591 cluster (cl, labeled with PDGFR α , red), at a time when the apical surface above the
592 cluster (labeled with EZRIN, green) remains flat. (B,C) Sections are stained with
593 phalloidin (white). Cluster-induced basal deformations are not seen in the absence of
594 mesenchymal clusters¹⁷ and can be easily discerned in phalloidin-stained sections. Lines
595 show the points of measurement of epithelial cell height over (red) and adjacent to (blue)
596 basal deformations caused by clusters (cl). Some sections that were used for
597 measurement were co-stained with the cluster marker, PDGFR α . Scale bar = 20 μ m. (D)
598 Box and whisker plots comparing epithelial cell height over mesenchymal clusters and
599 between clusters, showing the maximum, minimum, and median of the data sets. (E)
600 Comparison of cell volume over and between clusters ($p > 0.05$, unpaired t test). Error
601 bars represent standard deviation. (F) Quantification of epithelial nuclei per unit apical
602 surface (“Relative Cell Density”) above and between clusters ($p < 0.0001$, unpaired t
603 test). Error bars represent standard deviation. (G) Cross-section through the epithelium

604 (E-cadherin, white, and outlined) just after cluster formation. Bottom panels are
605 projections of the plane highlighted in green. Note that cells over clusters (outlined in
606 red) appear expanded circumferentially relative to cells between clusters (outlined in
607 blue). Scale bar = 15 μm .

608

609 **Figure 6. A computational model to investigate the forces involved in fold**
610 **development.** (A-D) FEM plots from the simulations run in Abaqus, with apical surface
611 emphasis added (dashed lines). The values of the vertical component of the displacement
612 correspond to the colors on the heat map. Line drawings above summarize the results. (A,
613 B) Compression from the clusters alone or in combination with a defect in stiffness to
614 represent a mitotic cell is insufficient to cause an invagination. (C) Addition of a vertical
615 contraction at a mitotic cell generates a fold with similar morphology to that observed *in*
616 *vivo* (compare with Figure 4, panel C). The combination of these three factors result in
617 cell division-mediated invaginations in the intestinal epithelium. (D) Cell rounding in the
618 absence of cell expansion results in a broader invagination that resembles V-shaped folds
619 (compare with Figure 4, panel B). Movies of these simulations are also provided
620 (Supplemental Movies 1-4).

621

622 **Figure 7. F-actin enrichment in mitotic cells located at T-folds.** (A) A mitotically
623 rounded cell at a T-fold, stained with phalloidin to mark F-actin. Note the tether of F-
624 actin (asterisk) from the base of the cell body to the basal surface. Also note that the top
625 of the cell body is well below the apical surface of the epithelium (internalized cell

626 rounding). (B) The same cell, with phalloidin in red and pHH3 in green. Scale bar = 20

627 μm .

628

629

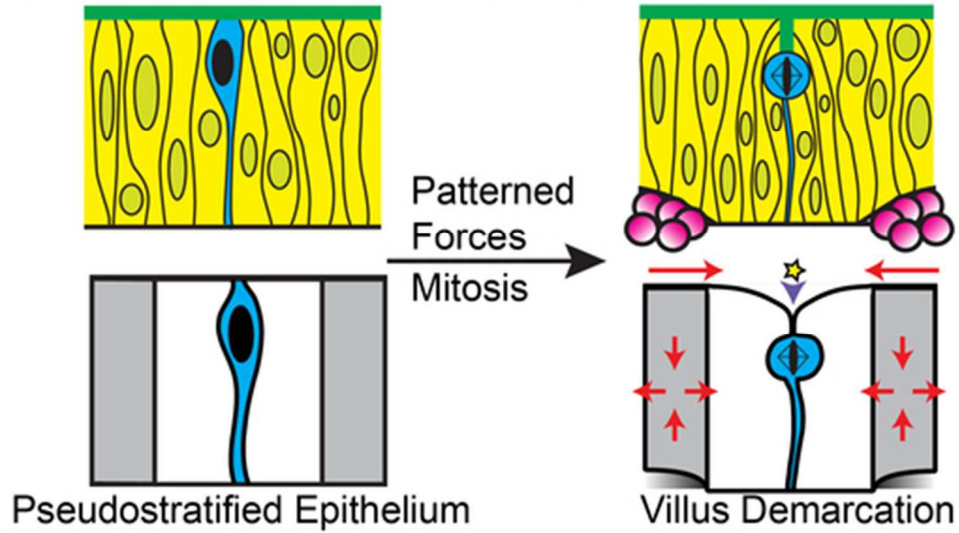
630

References

- 631 1 H. F. Helander and L. Fändriks, *Scandinavian Journal of Gastroenterology*, 2014,
632 **49**, 681–689.
- 633 2 M. Mathan, P. C. Moxey and J. S. Trier, *Am. J. Anat.*, 1976, **146**, 73–92.
- 634 3 P. C. Moxey and J. S. Trier, *The Anatomical Record*, 1979, **195**, 463–482.
- 635 4 J. L. Madara, *Comprehensive Physiology*, John Wiley & Sons, Inc., Hoboken, NJ,
636 USA, 2010.
- 637 5 C. Sauvanet, J. Wayt, T. Pelaseyed and A. Bretscher, *Annu. Rev. Cell Dev. Biol.*,
638 2015, **31**, 593–621.
- 639 6 O. Goulet, F. Ruemmele, F. Lacaille and V. Colomb, *J. Pediatr. Gastroenterol.*
640 *Nutr.*, 2004, **38**, 250–269.
- 641 7 O. Goulet and F. Ruemmele, *YGAST*, 2006, **130**, S16–28.
- 642 8 M. Stelzner and D. C. Chen, *Rejuvenation Research*, 2006, **9**, 20–25.
- 643 9 R. Clarke, *J Embryol Exp Morph*, 1967, **17**, 131–138.
- 644 10 J. M. Forrester, *J. Anat.*, 1972, **111**, 283–291.
- 645 11 M. A. Helmrath, W. E. VanderKolk, G. Can, C. R. Erwin and B. W. Warner, *J. Am.*
646 *Coll. Surg.*, 1996, **183**, 441–449.
- 647 12 T. Toyota, M. Yamamoto and K. Kataoka, *Arch. Histol. Cytol.*, 1989, **52**, 51–60.
- 648 13 A. S. Grosse, M. F. Pressprich, L. B. Curley, K. L. Hamilton, B. Margolis, J. D.
649 Hildebrand and D. L. Gumucio, *Development*, 2011, **138**, 4423–4432.
- 650 14 L. Karlsson, P. Lindahl, J. K. Heath and C. Betsholtz, *Development*, 2000, **127**,
651 3457–3466.
- 652 15 A. Kolterud, A. S. Grosse, W. J. Zacharias, K. D. Walton, K. E. Kretovich, B. B.
653 Madison, M. Waghay, J. E. Ferris, C. Hu, J. L. Merchant, A. A. Dlugosz, A. H.
654 Kottmann and D. L. Gumucio, *Gastroenterology*, 2009, **137**, 618–628.
- 655 16 K. D. Walton, A. Kolterud, M. J. Czerwinski, M. J. Bell, A. Prakash, J. Kushwaha,
656 A. S. Grosse, S. Schnell and D. L. Gumucio, *Proc. Natl. Acad. Sci. U.S.A.*, 2012,
657 **109**, 15817–15822.
- 658 17 K. D. Walton, M. Whidden, A. Kolterud, S. K. Shoffner, M. J. Czerwinski, J.
659 Kushwaha, N. Parmar, D. Chandrasekhar, A. M. Freddo, S. Schnell and D. L.
660 Gumucio, *Development*, 2016, **143**, 427–436.
- 661 18 M. Tawk, C. Araya, D. A. Lyons, A. M. Reugels, G. C. Girdler, P. R. Bayley, D. R.
662 Hyde, M. Tada and J. D. W. Clarke, *Nature*, 2007, **446**, 797–800.
- 663 19 C. E. Buckley, X. Ren, L. C. Ward, G. C. Girdler, C. Araya, M. J. Green, B. S.
664 Clark, B. A. Link and J. D. W. Clarke, *The EMBO Journal*, 2013, **32**, 30–44.
- 665 20 M. Nishimura, Y. Inoue and S. Hayashi, *Development*, 2007, **134**, 4273–4282.
- 666 21 T. Kondo and S. Hayashi, *Nature*, 2013, **494**, 125–129.
- 667 22 E. Hoijman, D. Rubbini, J. Colombelli and B. Alsina, *Nat Comms*, 2015, **6**, 7355.
- 668 23 T. J. Hughes, *The finite element method: linear static and dynamic finite element*
669 *analysis*, Courier Corporation, 2012.
- 670 24 R. G. Fehon, A. I. McClatchey and A. Bretscher, 2010, 1–12.
- 671 25 B. Monier, M. Gettings, G. Gay, T. Mangeat, S. Schott, A. Guarner and M. Suzanne,
672 *Nature*, 2015, **518**, 245–248.
- 673 26 Y. Yamaguchi, N. Shinotsuka, K. Nonomura, K. Takemoto, K. Kuida, H. Yosida
674 and M. Miura, *The Journal of Cell Biology*, 2011, **195**, 1047–1060.
- 675 27 Y. Yamaguchi and M. Miura, *Cell. Mol. Life Sci.*, 2012, **70**, 3171–3186.

- 676 28 T. Wang, K. Yanger, B. Z. Stanger, D. Cassio and E. Bi, *J. Cell. Sci.*, 2014, **127**,
677 2483–2492.
- 678 29 M. A. Schlüter, C. S. Pfarr, J. Pieczynski, E. L. Whiteman, T. W. Hurd, S. Fan, C.-J.
679 Liu and B. Margolis, *Molecular Biology of the Cell*, 2009, **20**, 4652–4663.
- 680 30 K. Taniguchi, Y. Shao, R. F. Townshend, Y.-H. Tsai, C. J. DeLong, S. A. Lopez, S.
681 Gayen, A. M. Freddo, D. J. Chue, D. J. Thomas, J. R. Spence, B. Margolis, S.
682 Kalantry, J. Fu, K. S. O’Shea and D. L. Gumucio, *Stem Cell Reports*, 2015, **5**, 954–
683 962.
- 684 31 G. M. Odell, G. Oster, P. Alberch and B. Burnside, *Developmental Biology*, 1981,
685 **85**, 446–462.
- 686 32 M. A. Gelbart, B. He, A. C. Martin, S. Y. Thiberge, E. F. Wieschaus and M.
687 Kaschube, *Proc. Natl. Acad. Sci. U.S.A.*, 2012, **109**, 19298–19303.
- 688 33 O. Polyakov, B. He, M. Swan, J. W. Shaevitz, M. Kaschube and E. Wieschaus,
689 *Biophysical Journal*, 2014, **107**, 998–1010.
- 690 34 E. Moeendarbary, L. Valon, M. Fritzsche, A. R. Harris, D. A. Moulding, A. J.
691 Thrasher, E. Stride, L. Mahadevan and G. T. Charras, *Nature Materials*, 2013, **12**,
692 253–261.
- 693 35 O. Brunser and J. H. Luft, *Journal of Ultrastructure Research*, 1970, **31**, 291–311.
- 694 36 L. Lu, S. J. Oswald, H. Ngu and F. C. P. Yin, *Biophysical Journal*, 2008, **95**, 6060–
695 6071.
- 696 37 H. K. Matthews, U. Delabre, J. L. Rohn, J. Guck, P. Kunda and B. Baum,
697 *Developmental Cell*, 2012, **23**, 371–383.
- 698 38 B. Li, Y. P. Cao, X. Q. Feng and H. Gao, *Journal of the Mechanics and Physics of*
699 *Solids*, 2011, **59**, 758–774.
- 700 39 K. Garikipati, *Applied Mechanics Reviews*, 2009, **62**, 030801–030801–7.
- 701 40 A. E. Shyer, T. R. Huycke, C. Lee, L. Mahadevan and C. J. Tabin, *Cell*, 2015, **161**,
702 569–580.
- 703 41 A. E. Shyer, T. Tallinen, N. L. Nerurkar, Z. Wei, E. S. Gil, D. L. Kaplan, C. J. Tabin
704 and L. Mahadevan, *Science*, 2013, **342**, 212–218.
- 705 42 B. Lacroix, M. Kedinger, P. Simon-Assmann and K. Haffen, *Gut*, 1984, **25**, 925–
706 930.
- 707 43 A. Matsumoto, K. Hashimoto, T. Yoshioka and H. Otani, *Anatomy and Embryology*,
708 2002, **205**, 53–65.
- 709 44 K. Nakamura and T. Komuro, *Journal of Electron Microscopy*, 1983, **32**, 338–347.
- 710 45 C. M. Dekaney, F. W. Bazer and L. A. Jaeger, *The Anatomical Record*, 1997, **249**,
711 517–523.
- 712 46 D. R. Burgess, *Development*, 1975, **34**, 723–740.
713

Murine intestinal villi are rapidly demarcated by patterned intraepithelial forces that are induced by mesenchymal cell clusters and accelerated by cell division.



45x27mm (300 x 300 DPI)